VTT Technical Research Centre of Finland

Design, manufacturing, and operation of movable 2 × 10 kW size rSOC system

Saarinen, Ville; Pennanen, Jari; Kotisaari, Mikko; Thomann, Olivier; Himanen, Olli; Iorio, S. Di; Hanoux, P.; Aicart, J.; Couturier, K.; Sun, X.; Chen, M.; Sudireddy, B. R.

Published in:
Fuel Cells

DOI:
10.1002/fuce.202100021

Published: 01/10/2021

Document Version
Publisher's final version

Received: 27 March 2021 | Revised: 3 September 2021 | Accepted: 16 September 2021

DOI: 10.1002/fuce.202100021

Fuel Cells
From Fundamentals to Systems

ORIGINAL RESEARCH PAPER

Design, manufacturing, and operation of movable 2 × 10 kW size rSOC system

V. Saarinen D.Sci. (Tech.)[1] | **J. Pennanen MSc**[1] | **M. Kotisaari MSc**[1] | **O. Thomann D.Sci. (Tech.)**[1] | **O. Himanen D.Sci. (Tech.)**[1] | **S. Di Iorio PhD**[2] | **P. Hanoux DUT**[2] | **J. Aicart PhD**[2] | **K. Couturier PhD**[2] | **X. Sun PhD**[3] | **M. Chen PhD**[3] | **B. R. Sudireddy PhD**[3]

[1] VTT Technical Research Centre of Finland, Espoo, Finland

[2] Univ. Grenoble Alpes – CEA/LITEN, Grenoble, France

[3] Anker Engelunds Vej, Technical University of Denmark, Lyngby, Denmark

Correspondence
V. Saarinen, VTT Technical Research Centre of Finland, Tietotie 4C, FI-02150 Espoo, Finland.
Email: ville.saarinen@vtt.fi

Funding information
BALANCE EU, Grant/Award Number: 731224

Abstract

Reversible solid oxide cell (rSOC) technology enables both electricity generation for local demands and electricity conversion into hydrogen with high power-to-gas (AC to H_2) efficiency. This work describes modeling and implementation of movable "10-feet container" size rSOC system in a pilot demonstration scale (10 kW SOEC/2 kW SOFC). The selected two-stack two-module system layout is the simplest option to investigate multi-module rSOC systems in various operation modes and conditions. Special attention is also paid to heat integration: heat losses are minimized with optimized BoP component design, placement, and insulation. Reversibility, dynamic operation, and methods for efficient transitions between SOFC and SOEC modes are investigated at a system level. The developed system is highly instrumented enabling detailed system analysis, for example, the calculation of enthalpy flows and efficiencies of all BoP components. Analyses of key parameters on the performance and efficiency are presented. To explore upscaling of rSOC systems, the effects of size and structure of stack modules on the reliability and maintenance of the entire system are investigated, and as a conclusion, the construction of multi-MW scale rSOC systems are recommended to be implemented with approximately 100 kW size stack modules.

KEYWORDS

electrolyzer, fuel cell, hydrogen production, power-to-gas, power-to-X, reversible high temperature solid oxide cell system, rSOC, SOEC, SOFC, solid oxide electrolyzer cell system, solid oxide fuel cell system

1 | INTRODUCTION

Mitigation of climate change and finding ways for greenhouse gas (especially CO_2) emission reductions are among the greatest challenges of our time. Hydrogen as a carbon-free fuel and possessing the highest energy density per mass (142 MJ/kg HHV) compared to any other fuel, will very likely be part of future energy systems, which also must meet the requirements of being both carbon-free and renewable [1]. Further on hydrogen energy systems, where hydrogen acts both as fuel and energy storage vector, are playing a key role in ongoing energy transition and decarbonization [2,3].

Nowadays around 96% of hydrogen is produced with fossil fuels, mainly with steam methane reforming (SMR) and remaining 4% by water electrolysis [4,5]. Because of environmental reasons, there is a growing motivation to develop different water electrolysis technologies: alkaline (AEL), proton exchange membrane (PEM), solid oxide electrolysis (SOE) [6,7], and other methods for green hydrogen production [8]. Many studies have recently been done concerning sustainable large-scale clean hydrogen production and storage, for example, see [5,9,10]. Also, practical level scenarios with techno-economic assessments and feasibility studies have been developed, for example, combining wind power plants to hydrogen storage [11] and study showing that in the long-term storage (>100 h), the hydrogen systems are more efficient compared to electric storage [12].

Power-to-gas concepts with hydrogen storage can contribute to the intermittent nature of renewable energy sources in many time scales by producing hydrogen during excess electrical generation and generating electrical power with high efficiency with fuel cells, when there is not enough wind or solar energy available [11,13,14]. The fuel cell technology is highly efficient to transform both fossil and clean fuels into the combined heat and power (CHP) [15] and the potential for the highest system efficiency among them has the reversible solid oxide cell (rSOC) technology [16,17].

Altogether, the motivation for developing the rSOC system described in this paper are rising from three conclusive advantages, which the rSOC technology is having compared to the other technologies: (a) potential for very high AC to H_2 system efficiency (80-90%) without polluting emissions; (b) Reversibility, that is, the same system can work both as a fuel cell and an electrolyzer depending on the power generation and grid stabilization needs; (c) Fuel flexibility and CHP in fuel cell mode and capability of co-electrolysis of steam and CO_2 in electrolysis mode, which enables very efficient power-to-X, if integrating rSOC systems as a part of industrial processes.

Even though the rSOC technology [16,17] is a very promising and potential technology, it still needs further development (longer lifetime, lower price) to reach full commercial phase such as PEM [18] and alkaline [19] technologies. Some rSOC proof of concepts and operational system results have been reported during recent years, for example, by Sunfire GmbH [20–23] and Sylfen [24,25]. This paper is concentrated on system-level studies as a continuum for our previous works of rSOC stack characterization, performance, and durability analysis [26,27].

2 | EXPERIMENTAL SECTION

2.1 | Design targets for reversible solid oxide cell system

While the stack level research concentrates to optimize the stack level efficiency in standardized conditions, the system-level research objective is the system operation as close as possible to the real end-user conditions. The selected two-stack two-module system layout is the simplest option to investigate multi-module rSOC systems in various operation modes and conditions. That is the optimal way to get design and operation experiences, which can be applied for larger multi-module (>1-10 MW) systems. The summarized design targets for VTT's rSOC system were:

(i) "10 feet container" size movable rSOC pilot system
(ii) Modular system layout, where the stack modules are connected to the common BoP part
(iii) Optimized heat integration in means of insulation, component placement, and waste heat recovery
(iv) AC electricity supply to the local (in-house) electricity network and measurement signal digitalization using Modbus RTU protocol
(v) Efficiency targets in system level: 50% in fuel cell mode and 90% in electrolysis mode
(vi) Achieve the reversibility and dynamic operation at the system level

2.2 | The rSOC system level modeling and efficiency

The rSOC system design was done with 3D FEM modeling. A stationary Matlab-Simulink system model was developed as well as the physical models for the BoP components. The fuel cell operation was designed for 100% hydrogen as a fuel and the electrolysis operation for the steam

electrolysis. The system design was made according to the operating temperature range of 700–800 °C.

The most interesting SOEC mode variable at the system level is the AC to H_2 efficiency. The efficiency is naturally dependent on the operating point used and is therefore not constant. It is often given only one value for the system efficiency, which usually represents the maximum efficiency value under conditions where the long-term operation of the system is still possible. In practice, this means that the reported system-level efficiency is related to the operating point at which the highest utilization rate of steam is used. In addition to this, the typical operating point usually has the current density at which the average cell voltage of the stack is slightly above the so-called thermoneutral voltage, which in this case is about 1.285 V.

The AC to H_2 system-level efficiency of the SOEC is usually given according to the HHV of hydrogen, which can be justified because the commercial value of the produced hydrogen is usually determined by its HHV value. Since the fuel cell mode efficiencies are often reported based on the LHV value of the fuel, it is also useful to report the AC to H_2 efficiency calculated using the LHV value, which is also needed when calculating the power-to-power round trip efficiency of the rSOC system, which is in reality only around 30-40%.

If the rSOC system will be used for the electrolysis, where the steam is freely available, for example, as a by-product of industrial processes, for these applications the measured AC to H_2 efficiency can be reported in such a form that does not take into account the power consumed for the steam production. Usually, this result is calculated by assuming a temperature of freely available steam of 150° C. In this case of freely available steam, the most economically optimal operating point can also be found at some lower steam utilization rate. Thus, the system level AC to H_2 efficiency is defined according to Equation (1):

$$\eta_{AC\,to\,H_2}(HHV\ or\ LHV) = \frac{HHV\ or\ LHV\ of\ produced\ H_2}{Total\ AC\ power\ input} \quad (1)$$

where the Total AC power input is a sum of three separate terms: AC power input for electrolysis + AC power input for heaters + AC power input for evaporator. The AC power input for electrolysis includes all AC power consumed by the power supply. This term also includes the voltage losses outside the stack, the power consumption of the power source, and the AC/DC conversion efficiency. The total AC power input does not contain a separate term for the power consumption of the other BoP components, since this rSOC system has no pumps or blowers. Airflow is based on compressed air and the other gas flows are based on above ambient inlet pressure. In this analysis, the amount of hydrogen produced is calculated from the current by assuming a 100% Faradic efficiency. Since the rSOC system does not have a hydrogen storage unit, the system level AC to H_2 efficiency is calculated by assuming that the produced hydrogen is stored at atmospheric pressure.

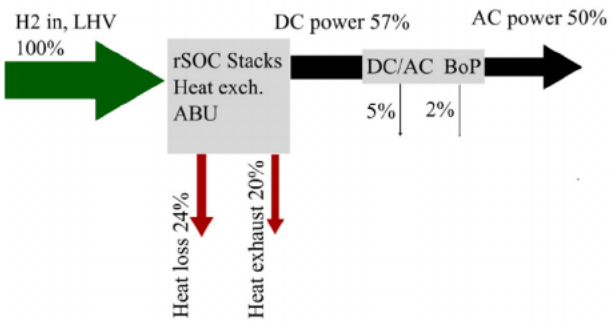

FIGURE 1 SOFC H_2-to-AC efficiency is 50% (LHV)

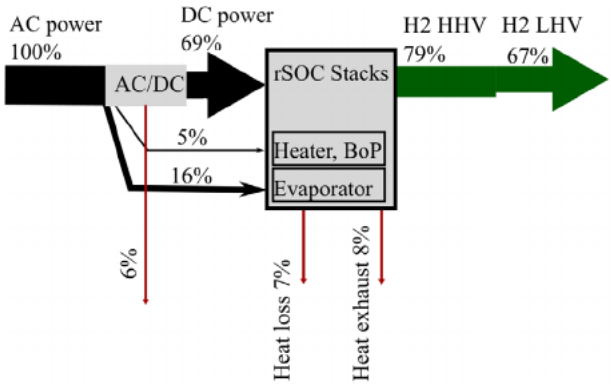

FIGURE 2 SOEC AC-to-H_2 efficiency is 67% (LHV), if steam production included

The selected SOFC and SOEC nominal operation points are described below. The hydrogen to DC electricity (H_2-to-DC) conversion efficiency in the stack level is 57% (LHV). With all DC-to-AC conversion-related effects added, the overall H_2-to AC conversion efficiency is estimated to be 50% (LHV; Figure 1). The AC-to-H_2 efficiency is 67% when calculated with lower heating value (LHV) and 79% when calculated with a higher heating value (HHV) (Figure 2). If there is freely available steam for the rSOC system, for example, from the power plant or from the industrial process, the electrical energy required to produce 100 °C steam from 10° C water can be excluded from the electrical input. Then the corresponding DC-to-H_2 efficiency values are 86% (LHV) and 102% (HHV). With this assumption and with AC-to-DC conversion added, the overall AC-to-H_2 efficiency is 80% when calculated with the lower heating value (LHV) and 94% when calculated with the higher heating value (HHV). Those values are then determining the following nominal operation points for the rSOC system design. Selected SOFC nominal operation point:

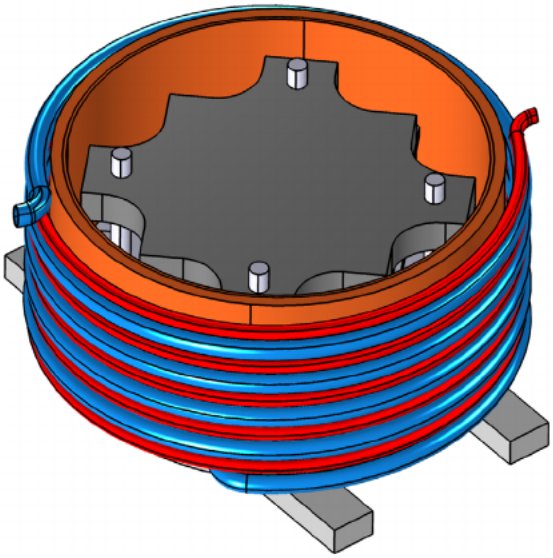

FIGURE 3 Stack module including coiled gas preheating tubings around the electrical heater

(i) Fuel gas composition: 100% H_2
(ii) Fuel utilization $U_f = 80\%$
(iii) Current density $i = 0.4$ A cm^{-2}
(iv) $T_{stack\_outlet} = 700\,°C$
(v) H_2-to-AC efficiency: 50% (LHV)
(vi) H_2-to-AC efficiency: 43% (HHV)

Selected SOEC nominal operation point:

(i) Inlet gas composition $H_2/H_2O = 10/90$
(ii) Steam conversion SC = 80%
(iii) Current density $i = 1$ A/cm^2
(iv) $T_{stack\ inlet} = 700°C$
(v) $T_{stack\ outlet} \geq 700\,°C$
(vi) AC-to-H_2 efficiency (steam production included): 67% (LHV), 79% (HHV)
(vii) AC-to-H_2 efficiency (steam production excluded): 80% (LHV), 94% (HHV)

The system modeling strongly indicated that the rSOC system cannot be designed to be in heat balance in the electrolysis mode with only the heat production of the stacks, which does not compensate the heat losses in a system of this scale. The needed current density would be too high for the state-of-the-art SOE cells and it would significantly increase the cell degradation. Thus, the cylinder-shaped electrical heaters were designed around both two stacks of the rSOC system. Inlet air and inlet steam/hydrogen pipes were formed into spirals around each electrical heater (Figure 3). These heaters heat the stacks as well as the incoming gases during both the start-up of the system or transitions between SOFC and SOEC modes and during the endothermic operation in the SOEC

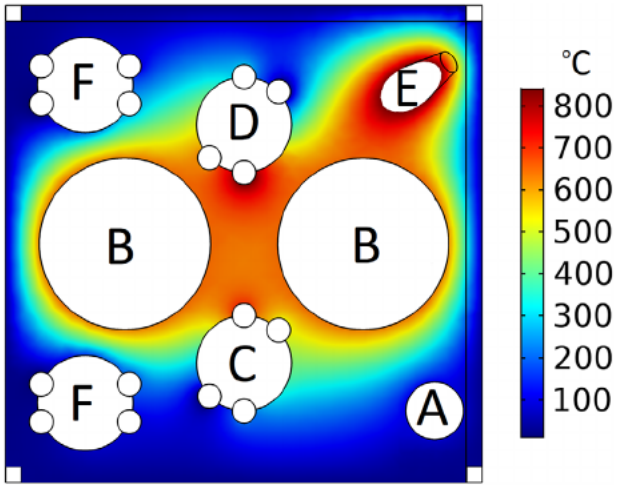

FIGURE 4 Temperature distribution of the thermal insulation material inside the hot box and locations of the main BoP components: The evaporator for steam production (a), two electrical band heaters for the stack modules (b), heat exchangers for the fuel side (c) and the air side (d), the catalytic afterburner (e) and outlet gas coolers (f)

mode. The electrical power needed to increase the temperature of the stack inlet gases was having about 5% effect on the system efficiency in the electrolysis mode.

2.3 | Balance-of-plant components

The size of the rSOC system hot box is about 1 m^3 and locations of the main BoP are presented in Figure 4: The evaporator for the steam production (A), the two electrical band heaters for the stack modules (B), the heat exchangers for the fuel side (C) and the air side (D), the catalytic afterburner (E) and the outlet gas coolers (F). The heat losses of the rSOC system were minimized and BoP component placements were optimized using the developed 3D temperature model. One of the most important design principles of the rSOC system was that the mutual placement of the BoP components and their interconnecting pipes were implemented so that the heat losses of the hottest components of the system (the catalytic afterburner and the stack modules) could be utilized by the other BoP components of the system or the connecting pipes.

Instead of isolating all individual BoP components and pipes, the rSOC system was thermally insulated by filling the entire volume of the hot box with ceramic granular thermal insulation material. The selected insulation method enables excess heat utilization for the internal use of the rSOC system but prevents the heat losses from the stack modules and individual BoP components into the environment. The temperature distribution of the hot box was estimated with the information from the developed

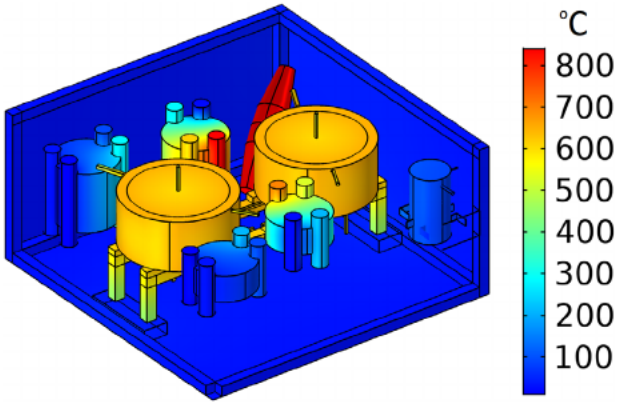

FIGURE 5 The rSOC hot box and example of surface temperature distribution of BoP components in SOEC mode

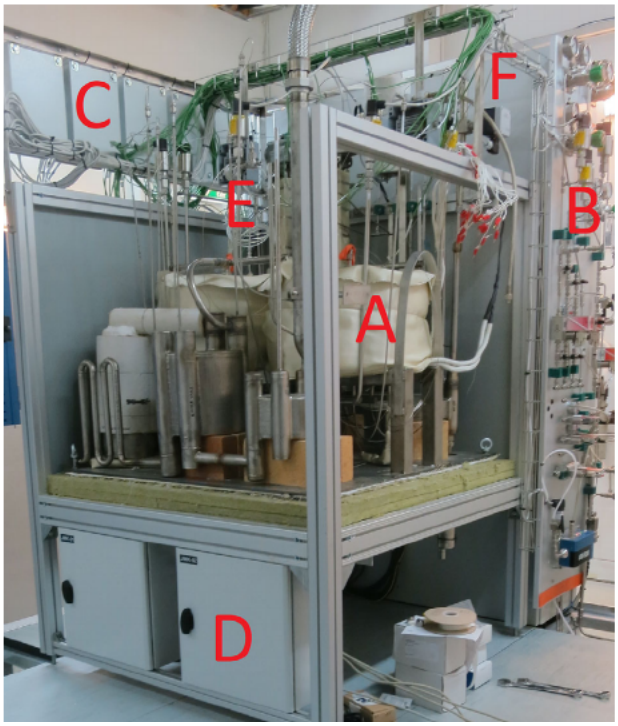

FIGURE 6 Main parts of the rSOC system: Insulated stack modules (a), Gas supply control (MFCs, valves) (b), Cupboards for power supply, relays and measurement signal interfaces (c), Stack instrumentation interface boxes (d), Measurement signal (T,p,U) wirings (e), and PLC cupboard (f). Power electronics (bidirectional load units) are placed under the hot box

system model. One example of the surface temperature distribution of the BoP components in the SOEC mode is presented in Figure 5. According to the 3D temperature modeling results, the overall heat loss from the hot box was estimated to be about 500 W. This is to be considered as the minimum heat loss. The main components of the rSOC system can be seen in Figure 6. The power electronics (bidirectional load units) are installed under the hot box. Gas supply control wall is on the right and the cupboards for the PLC are behind and the power supply and relay cupboards are on the left. In the case of an emergency, the uninterruptible power supply (UPS) would keep the logic control and the critical gas valves powered.

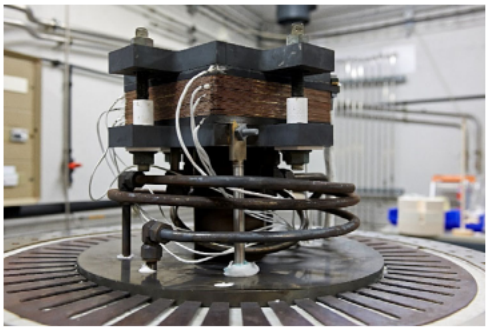

FIGURE 7 A CEA 25-cell stack with its self-clamping system after conditioning and quality check at CEA

2.4 | Solid oxide cells and stacks

In the EU project BALANCE (H2020 731224) the novel rSOC cells and stacks were developed by DTU and CEA, respectively. The cell architecture consists of Ni-yttria stabilized zirconia (Ni-3YSZ) fuel electrode support (ca. 300 μm), Ni-8YSZ fuel electrode (ca. 10 μm), YSZ electrolyte (ca. 10 μm), CGO barrier layer (ca. 6 μm), LSC-CGO ($La_{0.6}Sr_{0.4}CoO_{3-\delta}$-$Ce_{0.8}Gd_{0.2}O_{2-\delta}$) composite oxygen electrode (ca. 30 μm), and LSC contact layer (ca. 30 μm). The support layer, fuel electrode, electrolyte, and CGO diffusion barrier layer were fabricated using the tape casting method and co-sintered at ca. 1,300 °C. The sintered electrode supported cells were cut into the size of 120 mm × 120 mm (having 100 mm × 100 mm active surface area) using laser cutting. Subsequently, the LSC-CGO oxygen electrode was screen printed on the CGO barrier layer and sintered at ca. 950°C. Finally, the LSC contact layer was screen printed on the LSC-CGO oxygen electrode and sintered in air at ca. 950°C. The additional information on cell development can be found in previous works [28–30].

The 25-cell stacks using DTU electrode-supported cells were produced at CEA to be integrated into the VTT rSOC system. The stacks were first assembled, conditioned in the CEA test bench, and electrochemically characterized as a quality check (Figure 7). The CEA stack design was initially developed for the SOEC operation, but recently upgraded for the reversible SOFC/SOEC operation, with a particular emphasis on the decrease of the pressure drops especially on the air side. The planar stack with cross-flow fields was composed of thin interconnects using 0.2 mm AISI441 ferritic stainless steel sheets with in-plane inter-

FIGURE 8 Movable "10-foot container" size rSOC system

connect dimensions of 205 × 205 mm^2 and two thick endplates. Contact elements have been added between the interconnects and the cells with the same size as the electrodes: a nickel-mesh (100 meshes cm^{-2}) on the hydrogen side and an LSM contact element on the oxygen side. The sealing material was ceramic glass Schott G018-311 and a mica foil was used to ensure the electrical insulation between two adjacent interconnects, but also to complete the sealing. Additionally, a self-clamping system is placed around each stack for easy and safe transportation and integration of the stack into the rSOC system. Additional information on the stack design and the experimental results on performance, durability, and the gas conversion rates can be found in previous works [31–37].

2.5 | Automation system digitalization and data processing

The rSOC system (Figure 8) was designed to be highly instrumented having altogether more than 250 measurement variables like mass flow controllers (8), gas valves (10), bidirectional loads (2), humidity (2), pressure (13), and temperature (30+) measurements, cell voltages (50+) etc. Both rSOC system modules have separate bidirectional load/power source units (Elektro-Automatik EA-PSB 9080-2403U, 10kW), which provide AC electricity in local (in-house) electricity network when operating in the SOFC mode. The system operation was controlled and monitored with the developed automation PLC (programmable logic controller) system. The more than 250 measurement variables were enabling detailed system analysis and e.g. the calculation of enthalpy flows and efficiencies of all individual BoP components separately. For the developed rSOC system, the digitalization of control and measurement signals were implemented with the Modbus RTU / TCP protocol, providing better reliability, higher accuracy, more developed signal processing, smaller size, and reduced signal noise compared to previously used analog measured signals.

3 | RESULTS AND DISCUSSION

3.1 | Heat-up and stack level performance

The rSOC system testing was started with safety tests and leakage measurements followed by slow (1°C min^{-1}) system heating to 700°C. It was observed that all BoP components and rSOC system in general were working as planned. Also, the measured heat losses were very similar to the calculated ones. The only deviation was that during heat-up after 300 °C, some failures were observed with the another stack. During the first days of operation, iV-curves were measured in both SOFC and SOEC modes. Stacks were showing very similar behavior and performance values as tested by CEA: difference in $V_{cell\ mean}$ <5%, at 0.4 A cm^{-2}, even though relative high-performance variations were observed between the best and worst-performing cells (~100-200 mV at 0.4 A/cm^2). Those performance variations between individual cells were not connected to their locations in the stacks. Deeper performance analysis of these experimental stacks and individual cells was excluded from this study. After the first tests, the developed rSOC system was running in various operation conditions altogether more than 5000 h. During that time, the reversibility and dynamic operation (i.e., transitions between SOFC and SOEC modes) were investigated at the system level and multi-module rSOC system operation was demonstrated.

3.2 | AC to H_2 system-level efficiency

The system-level AC to H_2 efficiency values were calculated according to Equation (1) and those four different AC to H_2 efficiency values are presented in *Table 1*. The operating point for determining the AC to H_2 system-level efficiency value was with 80.8% steam utilization, an average cell voltage of 1.337 V, and a stack temperature of 750° C. The 63 A current was used for this measurement, which corresponds to an average current density of 0.63 A/cm^2. That current density was chosen, because it gave exactly the thermoneutral cell voltage (1.285 V). This required

TABLE 1 The rSOC system level efficiencies

rSOC system level	AC power for steam production included	Free 150 °C steam flow assumed
AC to H_2 efficiency (HHV)	71%	81%
AC to H_2 efficiency (LHV)	60%	69%

Abbreviations: AC, alternating current; rSOC, reversible solid oxide cell; HHV, higher heating value; LHV, lower heating value.

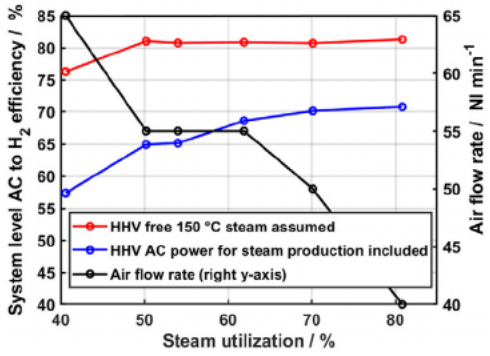

FIGURE 9 AC to H_2 system-level efficiencies as a function of steam utilization

current value was determined with a significantly lower (40%) steam utilization rate, whereas to maximize the efficiency, the steam and airflow rates were reduced to as low level as possible for the continuous operation.

The system performance was also measured using six other stationary operating points: the steam flow rate was varied over a period of two days so that the utilization rate of the steam increased gradually from 40% to 81%. Because the steam flow rate decreased also the pressure drop on the fuel side of the stacks, this parameter substantially decreased during the test. Also, the airflow rate had to be gradually reduced in order to keep the difference in pressure levels between the air and fuel inlets of the stack below the limit recommended by the stack manufacturer. The AC to H_2 system-level efficiency as a function steam utilization is presented in Figure 9, where it can be clearly seen that the efficiency improves, when lowering the gas flow rates. This result is as expected, since increasing the utilization rate of the steam reduces simultaneously the AC power required for the steam production. For the same reason, the efficiencies of the free steam cases do not change noticeably, when steam flow rate is reduced.

The observed improvements in efficiency with decreasing gas flows are due not only to a reduction of the AC power required to produce steam but also the AC power needed to heat the stack modules, since a significant part of the power consumed for stack modules heating is used to heat the inlet gases. Based on these results, the importance of the *AC power input for heaters*, which depends

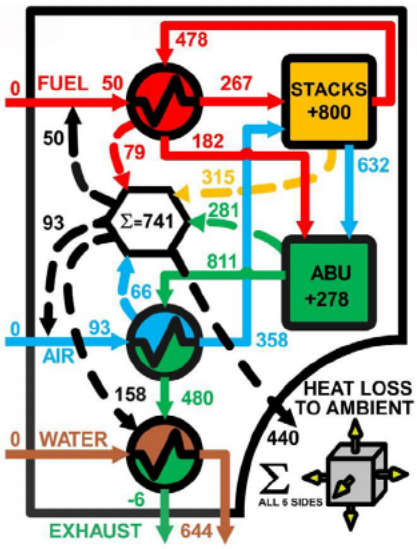

FIGURE 10 Enthalpy flow rates inside rSOC system at OCV in SOFC mode

only on the power used by electric heaters, is significantly less important in terms of efficiency than AC power input for the evaporator, which is related to the steam production. This conclusion can be done, since the effect of the power consumption of the heaters is included in the calculation of the efficiency of the free steam cases, and yet the efficiency of the free steam cases remains almost constant, when the steam utilization is above 50%.

3.3 | Enthalpy flows and system-level performance

The advantage of the highly instrumented rSOC system is that it can provide detailed measurement data across the entire system. Direct real-time measurement data can be used not only for the real-time monitoring and control of the system, but also for the advanced fault diagnostics. An example of the data-based model depicting the entire rSOC system is the system-wide enthalpy flow map (in one selected stationary state operating point) presented in Figure 10. The measured and calculated values of the process parameters like molar flow rates and both compositions and temperatures of the gas flows are required to calculate the corresponding enthalpy flows. From these enthalpy flow values, heat losses of each BoP component in the system (and associated pipings) and corresponding BoP component efficiency values can be calculated. Also, the thermodynamic couplings between the BoP components of the rSOC system can be then evaluated accordingly.

In Figure 10, the "virtual heat storage" is depicted in the middle with incoming arrows indicating the amount

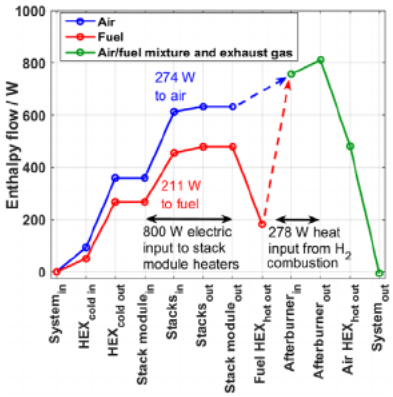

FIGURE 11 An example of enthalpy flows through rSOC system

of heat loss from each BoP component (66 W from air heat exchanger, 79 W from fuel heat exchanger, 281 W from afterburner and the 315 W represents the combined heat loss from both stack modules). Thus, the total amount of heat losses transferred for internal use of the system was 741 W. The black outward arrows represent outward heat flows from the virtual heat storage. The enthalpy flow map provides a comprehensive overview of system-wide enthalpy flow (especially for enthalpy flows along the out-of-pipe paths) and it is possible to do also more accurate and visually easier analysis, like presented in Figure 11.

3.4 | Heat loss analysis based on surface temperature measurements

Heat losses Affect the overall rSOC system efficiency and have also a significant role on the system level in these relatively small size systems. That is the case especially in SOFC mode, where the heat losses are having a more drastic impact on the system efficiency, since the produced AC power in SOFC mode is typically three to five times smaller than the consumed AC power in SOEC mode. The results presented in the previous subsections are indicating that the heat losses of the built rSOC system are quite close to the heat loss estimates used during the system design phase. However, it is worthwhile to investigate this issue also by direct measurements from the outer surface of the system, as there is a lot of empirical evidence that solutions that are considered to be quite insignificant during the construction phase of the system can have a significant effect on the overall system heat losses.

The surface temperature of the rSOC system hot box was measured from several points using thermocouples, having a maximum surface temperature value of 51°C. The measured temperature values and their locations were applied as a point constrains into a 2D heat transfer model resulting total heat loss of 440 W for the complete rSOC system. There are still some supporting structures that are not included in these values, but those are typically only a few degrees above the ambient temperature and can be neglected.

3.5 | Discussion and remarks concerning upscaling of kW size rSOC systems

It is quite clear that large MW size rSOC systems (about 200 times larger than the rSOC system presented in this paper) cannot be technically or economically just built by scaling up. The biggest technical challenge to direct upscaling would be the implementation of piping to hundreds of stacks to ensure a uniform distribution of the gas flows. Important topic is also the optimal number of stacks inside one modular unit. If one modular unit would have e.g. 200 stacks, it would be challenging to operate that system without interruptions with any realistic probability of a single-stack failure. In this example case, the assumed probability of failure of a single 1 MW system is almost 90%, if the probability of failure of a single stack is 1%, which is a realistic estimation according to the wide testing of current state-of-the-art SOE stacks. Thus, it is recommended to build MW scale systems from smaller modular units.

In terms of the physical size of the system, the implementation of the piping and the heat balance of the system, the upper limit for the number of stacks per unit would be in the range of 10. The power electronics, and in particular the efficiency of the DC/DC conversion is in a key role when optimizing the size of the modular stack units. A typical power electronics DC voltage level of applications for rSOC systems is about 400–600 V, so for a good DC/DC efficiency, the voltage produced by one modular unit should be in that order of magnitude. This gives us the number of cells needed for one modular unit. For example, at 600V with a 1.3V cell voltage (SOEC nominal operation point, just above the SOEC thermoneutral voltage) would mean 462 cells connected in series.

The largest SOE stacks currently in use have about 60–120 cells, so a modular unit of 462 cells could be implemented with 4–8 stacks. For example, in a six-stack unit, a single stack would have 77 cells, which is the appropriate size range for the technical and economic implementation of the stack. A system of this size can be implemented using electrically isolated gas distribution manifolds designed by VTT. The starting point for this scale-up review was to scale the current 2 × 10 kW rSOC system to 1 MW. In most grid-scale energy storage or power-to-X designs, the required electrolyzer power is from 10 MW to 100 MW, but even in these cases, using 100 kW building blocks may be a more reasonable option for system reliability and maintenance logistics than using bigger 1 MW modular units.

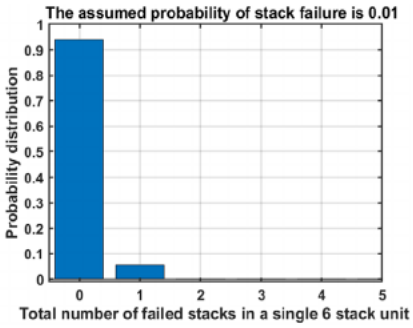

FIGURE 12 The probability distribution for the number of faulty stacks for 100 kW SOEC unit, which is assembled using six stacks

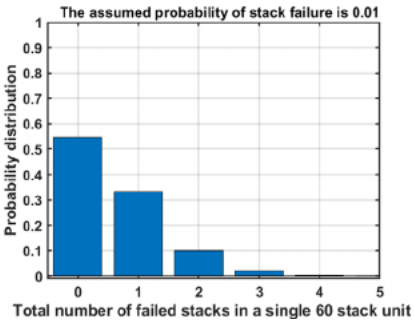

FIGURE 13 The probability distribution for the number of faulty stacks for 1 MW SOEC unit made by using 60 similar stacks as in 100 kW case

One important reason for keeping the number of stacks low in modular units is the lower failure probability of a single modular system compared to larger units. In both cases, which are presented in Figures 12 and 13, the failure probability of a single stack is assumed to be 1%. The simulation method used here is a classical binomial distribution, which requires the number of stacks in a modular system and the probability of failure of a single stack. How serious the failure is or how long the time window is used to determine the probability of failure is irrelevant in these cases, that is, they can be defined according to the issue under consideration. The failure probability of 1% is used to represent the order of magnitude, what the single-stack failure probability is recommended to be, when implementing the MW scale systems. If a small modular unit fails (for whatever reason), its importance for the overall operation of the system is negligible and can then easily closed and replaced by a corresponding unit with a non-urgent schedule. The small modular unit size also allows system-wide maintenance (including scheduled stack replacement) without the need to shut down the entire plant for maintenance.

In Figure 12, the single 100 kW modular unit had a failure probability of about 6%, whereas the 1 MW unit assembled from the corresponding stacks has a probability of failure of about 45% (Figure 13). For each 1 MW system constructed (10 units of 100 kW are required to build 1 MW system), the probability of failure of at least one single stack is the same (approximately 45%), because the total number of stacks is the same. However, in the case of a 1 MW modular unit, the significance of a single modular unit failure is completely different for the operation of the entire system (100% of the total system power is lost versus 10%). For a larger, for example, 10 MW system, the difference noted above is smaller but still significant. With these assumptions, the probability of losing more than 10% of the system's maximum power for a 10 MW SOEC built from 1 MW modules is about 98% and if built from 100 kW modules, only about 3%.

4 | CONCLUSION

The reversible high-temperature solid oxide cell (rSOC) system was modeled and implemented in a pilot demonstration scale (10 kW SOEC/2 kW SOFC). Special attention was paid to heat integration during the system design to minimize the heat losses with optimized BoP component design, placement, and insulation. Due to the high degree of instrumentation, the implemented rSOC system produced data for both system-wide analyses and from the operation of the individual BoP components. Based on the results obtained, the heat loss values of the individual BoP components measured from the actual system, as well as their performance, appeared to be very similar to those of the system model used during the design phase.

The measured rSOC system-level AC to H_2 efficiency (HHV, assuming free steam flow) was 81% in electrolyzer mode. In fuel cell mode, the H_2 to AC system-level efficiency could not be measured at the system nominal point due to the failure of another stack and partly due to the constraints imposed by the used pressure difference limits by the stack manufacturer. Operating pilot size rSOC system in challenging operating conditions was also giving valuable information, since larger systems are needed to be built from these smaller modular units. The developed rSOC system was running in various operation conditions altogether more than 5000 h. During that time, the reversibility and dynamic operation (i.e., transitions between SOFC and SOEC modes) were investigated at system level and multi-module rSOC system operation was demonstrated.

The extensive measurement data and derived quantities calculated from it can be used to determine system behavior in various operation conditions. Also, the same data can be used to develop a system model describing the existing system. Detailed modeling can be further used

to design larger rSOC systems based on similar types of solutions, which can also implement solutions that are not technically or economically feasible on the scale currently being implemented. According to the performed probability analysis e.g. the probability of losing more than 10% of the 10 MW size rSOC system's maximum power is 98%, if it is built from 1 MW modules, but only 3% if built from 100 kW modules. Scaling of the rSOC system now implemented, for example, to a system size of 100 kW SOEC/20 kW SOFC, that is, about 10 times the size of the current system, should be possible with the used structural solutions and potential megawatt-scale rSOC systems are recommended to be built from smaller modular units of that size.

ACKNOWLEDGMENTS

Reversible solid oxide cell, stack, and system research as a part of BALANCE EU project has been funded by H2020 under the grant agreement 731224. The development work for movable rSOC system has been done as a part of Finnish national Smart Otaniemi project.

LIST OF SYMBOLS AND ABBREVIATIONS

η	Efficiency / %
ABU	Afterburner
AC	Alternating current / A
AEL	Alkaline electrolysis
BoP	Balance of plant
CGO	Gadolinium doped ceria
DC	Direct current / A
FEM	Finite element method
FU	Fuel utilization / %
HHV	Higher heating value / MJ kg^{-1}
LHV	Lower heating value / MJ kg^{-1}
LSC	Lanthanum strontium cobaltite
LSM	Lanthanum strontium manganite
MFC	Mass flow controller
p	Pressure / Pa
PEM	Polymer electrolyte membrane
PLC	Programmable logic controller
rSOC	Reversible solid oxide electrolyser
RTU	Remote terminal unit
SC	Steam conversion
SMR	Steam methane reforming
SOEC	Solid oxide electrolyser cell
SOFC	Solid oxide fuel cell
T	Temperature / °C
TCP	Transmission control protocol
U	Voltage / V
UPS	Uninterruptible power supply
YSZ	Yttria-stabilized zirconia

REFERENCES

1. P. Nikolaidis, A. Poullikkas, *Renew. Sust. Energ. Rev.* **2017**, *67*, 597.
2. D. Parra, L. Valverde, F.J. Pino, M. K. Patel, *Renew. Sust. Energ. Rev.* **2019**, *101*, 279.
3. *The Future of Hydrogen report*, International Energy Agency, IEA, **2019**.
4. A. Al-Subaie, A. Maroufmashat, A. Elkamel, M. Fowler, *Int. J. Hydrogen Energy* **2017**, *42*, 19376.
5. I. Dincer, C. Acar, *Int. J. Hydrogen Energy* **2015**, *40*, 11094.
6. A. Buttler, H. Spliethoff, *Renew. Sust. Energ. Rev.* **2018**, *82*, 2440.
7. O. Schmidt, A. Gambhir, I. Staffell, A. Hawkes, J. Nelson, S. Few, *Int. J. Hydrogen Energy* **2017**, *42*, 30470.
8. I. Dincer, *Int. J. Hydrogen Energy* **2012**, *37*, 1954.
9. R.S. El-Emam, H. Özcan, *J. Clean. Prod.* **2019**, *220*, 593.
10. F. Zhang, P. Zhao, M. Niu, J. Maddy, *Int. J. Hydrogen Energy* **2016**, *41*, 14535.
11. B. Olateju, A. Kumar, M. Secanell, *Int. J. Hydrogen Energy* **2016**, *41*, 8755.
12. O.V. Marchenko, S.V. Solomin, *Int. J. Hydrogen Energy* **2015**, *40*, 3801.
13. P. Colbertaldo, S.B. Agustin, S. Campanari, J. Brouwer, *Int. J. Hydrogen Energy* **2019**, *44*, 9558.
14. M. Qadrdan, M. Abeysekera, M. Chaudry, J. Wu, N. Jenkins, *Int. J. Hydrogen Energy* **2015**, *40*, 5763.
15. H. Ammermann, P. Hoff, M. Atanasiu, J. Ayllor, M. Kaufmann, O. Tisler, *Advancing Europe's energy systems: stationary fuel cells in distributed generation*, FCH JU, **2015**.
16. M.B. Mogensen, M. Chen, H.L. Frandsen, C. Graves, J.B. Hansen, K.V. Hansen, A. Hauch, T. Jacobsen, S.H. Jensen, T.L. Skafte, X. Sun, *Clean Energy* **2019**, *3*, 175.
17. V. Venkataramanan, M. Pérez-Fortes, L. Wang, Y.S. Hajimolana, C. Boigues-Muñoz, A. Agostini, S.J. McPhail, F. Maréchal, J. Van Herle, P.V. Aravind, *J. Energy Storage* **2019**, *24*, 100782.
18. M. Carmo, D.L. Fritz, J. Mergel, D. Stolten, *Int. J. Hydrogen Energy* **2013**, *38*, 4901.
19. K. Zeng, D. Zhang, *Progress Energy Combust Sci* **2010**, *36*, 307.
20. K. Schwarze, O. Posdziech, S. Kroop, N. Lapeña-Rey, J. Mermelstein, *ECS Trans.* **2017**, *78*, 2943.
21. J. Mermelstein, O. Posdziech, *Fuel Cells* **2017**, *17*, 562.
22. K. Schwarze, O. Posdziech, J. Mermelstein, S. Kroop, *Fuel Cells* **2019**, *19*, 374.
23. O. Posdziech, K. Schwarze, J. Brabandt, *Int. J. Hydrogen Energy* **2019**, *44*, 19089.
24. A. Nechache, S. Hody, *ECS Trans.* **2019**, *91*, 2485.
25. M. Lamagna, B. Nastasi, D. Groppi, C. Rozain, M. Manfren, D.A. Garcia, *Energy Convers. Manag.* **2021**, *235*, 113993.
26. J. Tallgren, O. Himanen, M. Noponen, *ECS Trans.* **2017**, *78*, 3103.
27. M. Kotisaari, O. Thomann, D. Montinaro, J. Kiviaho, *Fuel Cells* **2017**, *17*, 571.
28. A. Hagen, P.V. Hendriksen, *ECS Trans.* **2017**, *78*, 145.
29. A. Hauch, K. Brodersen, M. Chen, M.B. Mogensen, *Solid State Ion.* **2016**, *293*, 27.
30. A. Hauch, M. Marchese, A. Lanzini, C. Graves, *J. Power Sources* **2018**, *377*, 110.
31. J. Mougin, A. Chatroux, K. Couturier, M. Petitjean, M. Reytier, G. Gousseau, F. Lefebvre-Joud, *Energy Procedia* **2012**, *29*, 445.
32. J. Mougin, A. Mansuy, A. Chatroux, G. Gousseau, M. Petitjean, M. Reytier, F. Mauvy, *Fuel Cells* **2013**, *13*, 623.

33. M. Reytier, J. Cren, M. Petitjean, A. Chatroux, G. Gousseau, S. Di Iorio, A. Brevet, I. Noirot-Le Borgne, J. Mougin, *ECS Trans.* **2013**, *57*, 3151.
34. S. Di Iorio, M. Petitjean, J. Petit, A. Chatroux, G. Gousseau, J. Aicart, M. De Saint Jean, J. Laurencin, M. Reytier, J. Mougin, *Proc. 11th European SOFC & SOE Forum* 2014, Lucerne, Switzerland, **2014**, pp. 1–8.
35. M. Reytier, S. Di Iorio, A. Chatroux, M. Petitjean, J. Cren, M. De Saint Jean, J. Aicart, J. Mougin, *Int. J. Hydrogen Energy* **2015**, *40*, 11370.
36. J. Aicart, S. di Iorio, M. Petitjean, P. Giroud, G. Palcoux, J. Mougin, *Proc. 13th European SOFC & SOE Forum* 2018, Lucerne, Switzerland, **2018**, pp. 1–11.
37. J. Mougin, S. Di Iorio, A. Chatroux, T. Donnier-Marechal, G. Palcoux, M. Petitjean, G. Roux, *ECS Trans.* **2017**, *78*, 3065.

How to cite this article: V. Saarinen, J. Pennanen, M. Kotisaari, O. Thomann, O. Himanen, S. Di Iorio, P. Hanoux, J. Aicart, K. Couturier, X. Sun, M. Chen, B. R. Sudireddy. *Fuel Cells*. **2021**, *21,* 477–487. https://doi.org/10.1002/fuce.202100021